Vol. 25, No. 3(2026) IA26853

Revista Mexicana de Ingeniería Química

Sustainable removal of Fe^{3+} and Pb^{2+} from water using *Agave americana* residue–based biomaterials: Adsorption performance and isotherm analysis

Remoción sostenible de Fe^{3+} y Pb^{2+} del agua mediante biomateriales basados en residuos de *Agave americana*: Desempeño de adsorción y análisis de isotermas

M.G. Contreras-Hernández[1,2*], J.E. Montoya-Badillo[2], I.N. Cordero-Soto[3], S. Valle-Cervantes[2], T.E. Lara-Ceníceros[4], J.C. Rojas-Montes[2,5], M.D.J. Rodríguez-Rosales[2], D. Reyes-Jáquez[2]

[1]*Tecnológico Nacional de México/ Instituto Tecnológico de Durango, Departamento de Ingenierías Química y Bioquímica, Blvd. Felipe Pescador 1830 Ote., Col. Nueva Vizcaya, 34080 Durango, C.P, Mexico / Estancias Posdoctorales para la Formación y Consolidación de las y los Investigadores por México SECIHTI.*

[2]*Tecnológico Nacional de México/ Instituto Tecnológico de Durango, Departamento de Ingeniería Química y Bioquímica, Blvd. Felipe Pescador 1830 Ote., Col. Nueva Vizcaya, 34080 Durango, C.P, Mexico*

[3]*Tecnológico Nacional de México/ Instituto Tecnológico de Durango, Departamento de Ingenierías Química y Bioquímica, Laboratorio Nacional CONAHCYT de Apoyo a la Evaluación de Productos Bióticos (LaNAEPBi), Blvd. Felipe Pescador 1830 Ote., C.P. 34080, Durango, Dgo., México.*

[4]*Centro de Investigación en Materiales Avanzados S. C. (CIMAV-Unidad Monterrey), Grupo de Materiales Avanzados Funcionales y Nanotecnología. Alianza Norte 202, Autopista Monterrey-Aeropuerto Km 10, Apodaca, Nuevo Leo?n, C.P. 66628 México.*

[5]*Investigador por México SECIHTI?TecNM/Instituto Tecnológico de Durango, Blvd. Felipe Pescador 1830 Ote., Col. Nueva Vizcaya, 34080 Durango, C.P, Mexico*

Received: April 15, 2026; Accepted: September 1, 2026

Abstract

Contamination of water resources by Fe and Pb remains a major environmental concern. This study evaluated untreated (BN), thermally treated (BT), ultrasound-treated (BU), and alkali-treated (BQ) biomaterials derived from *A. americana* leaf residues for the removal of metal ions from aqueous solutions. FT-IR analysis confirmed the presence of hydroxyl, carbonyl and carboxyl groups that may serve as potential adsorption sites. A full factorial design involving four biomaterials, two initial pH levels, and two particle sizes was used to compare adsorption performance under identical experimental conditions. Untreated BN exhibited the highest performance for the Fe(III) removal at pH 4 and 250 μm, reaching a maximum removal efficiency of 82.86%. In contrast, alkali-treated BQ achieved complete Pb(II) removal under at pH 5 and 250 μm. Equilibrium data for the iron BN system were best described by the Freundlich model, indicating heterogeneous adsorption, whereas Pb(II) adsorption onto BQ followed the Langmuir model, with a maximum adsorption capacity of 60.69 mg·g^{-1}. The main contribution of this work is the metal-specific selection of two biomaterials derived from the same residue, demonstrating that treatment effectiveness depended on the target metal ion. These findings support the valorization of *A. americana* residues as precursors for simple metal-specific bioadsorbents.

Keywords: Remediation, Adsorbent, Heavy metals, Lignocellulosic biomass, Environmental remediation.

Resumen

La contaminación de los recursos hídricos por Fe y Pb representa un importante problema ambiental. Este estudio evaluó biomateriales sin tratamiento (BN), tratados térmicamente (BT), mediante ultrasonido (BU) y alcalinamente (BQ), obtenidos de residuos de hojas de *A. americana*, para remover metales en soluciones acuosas. El análisis FT-IR confirmó la presencia de grupos hidroxilo, carbonilo y carboxilo como sitios potenciales de adsorción. Se empleó un diseño factorial completo con cuatro biomateriales, dos niveles de pH inicial y dos tamaños de partícula para comparar su desempeño bajo condiciones idénticas. BN presentó el mejor desempeño para el sistema de hierro a pH 4 y 250 μm, con una remoción máxima de 82.86%. En contraste, BQ alcanzó una remoción completa de Pb(II) en las condiciones de pH 5 y 250 μm. Los datos de equilibrio del sistema hierro BN se describieron mejor con el modelo de Freundlich, lo que indicó adsorción heterogénea, mientras que la adsorción de Pb(II) sobre BQ siguió el modelo de Langmuir, con una capacidad máxima de 60.69 mg·g^{-1}. La principal contribución fue la selección específica de dos biomateriales derivados de residuos de *A. americana*, demostrando que la efectividad del tratamiento dependió del ion objetivo.

Palabras clave: Remediación, Adsorbente, metales pesados, Biomasa lignocelulósicos, Remediación ambiental.

*Corresponding author. *E-mail*: mgorety@itdurango.edu.mx;
https://doi.org/10.24275/rmiq/IA26853
ISSN:1665-2738, *issn-e*: 2395-8472

1 Introduction

Water is essential for life, yet ensuring safe and sufficient supplies for a growing global population remains one of the most pressing environmental challenges. As reported by Sharma *et al*. (2024), approximately 97.5% of the planet's water is saline, leaving only 2.5% as freshwater. Of this fraction, only a small proportion is readily accessible for human use, with approximately 13% found in surface and subsurface sources, while most remains trapped in glaciers. Consequently, the availability of water for agriculture, livestock production, and domestic consumption depends not only on quantity but also on quality, which is increasingly compromised by contaminants associated with industrialization and mining activities (Syeed *et al*. 2023).

Water contamination by potentially toxic metals remains a major environmental and public health concern, particularly in regions affected by mining and industrial activities. Mining operations generate metal-rich residues that, under atmospheric and oxidative conditions, may promote acid mine drainage and facilitate the mobilization of metal ions into soils, groundwater, and surface water resources (Alcázar-Medina *et al*. 2020; Prasad *et al*. 2023). Although elements such as Fe, Co, Mn, and Cu are essential for biological functions at trace concentrations, excessive exposure may cause neurological, hematopoietic, renal, and reproductive disorders. In contrast, Pb, Cr, Cd, and As may exert toxic effects even at relatively low concentrations (Prasad *et al*. 2023; Santos *et al*. 2019). Their persistence, non-biodegradable nature, and potential for bioaccumulation further increase the risks posed to ecosystems and human health.

Among the technologies available for metal removal, adsorption has attracted considerable attention because of its operational simplicity, versatility, and compatibility with low-cost materials. In particular, lignocellulosic residues from agricultural, food, and beverage industries contain hydroxyl, carboxyl, carbonyl, and ether groups that can interact with metal ions through ion exchange, surface complexation, electrostatic attraction, and other physicochemical mechanisms. Their conversion into bioadsorbents also supports circular-economy strategies by reducing waste generation while producing value-added materials (Perez-Pimienta *et al*. 2024; Rathnayaka *et al*. 2024). Recent studies have demonstrated the potential of agricultural residues, including artichoke waste and Luffa cylindrica, as low-cost adsorbents for removing metal contaminants from aqueous solutions (Diaz-Rodriguez et al. 2025; Moreno-Rubio *et al*. 2025).

In Mexico, the tequila and mezcal industries represent economically important sectors but also generate considerable quantities of lignocellulosic residues. During beverage production, the central stem ("piña") is processed, whereas the leaves are generally removed and discarded. The limited utilization of this residual biomass has encouraged the development of sustainable alternatives for its valorization (Martínez *et al*. 2019; Pérez-Zavala *et al*. 2020). Agave leaves are therefore attractive precursors for bioadsorbent production because of their fibrous structure, local availability, and abundance of oxygen-containing functional groups associated with cellulose, hemicellulose, and lignin.

Previous studies have demonstrated the potential of different Agave species for water treatment. Fibers and modified leaves from *A. americana* have been evaluated for the adsorption of trivalent and hexavalent chromium, whereas cellulose isolated from this species has been used to prepare magnetic cellulose-based nanocomposites for fluoride removal (Majamo *et al*. 2024; Rathnayaka *et al*. 2024). Likewise, fibers obtained from *A. angustifolia* residues have achieved Pb(II) removal efficiencies of up to 90% (Flores-Trujillo *et al*. 2021), while cellulose nanofibrils derived from *A. tequilana* Weber var. Azul showed promising adsorption performance toward Pb(II) (Hernández-Francisco *et al*. 2020). Similarly, *A. salmiana* has been studied as a bioadsorbent for cobalt and cobalt-nickel ionic species in batch systems (López-González *et al*. 2022).

Although *A. tequilana* Weber var. Azul is the best-known Agave species in Mexico because of its use in tequila production, *A. americana* was selected for the present study because mature leaf residues are readily available in Durango region and remain comparatively underutilized. The selection of this species was based on regional availability and the opportunity to valorize a locally generated lignocellulosic residue rather than on an assumption of superior adsorption performance. Furthermore, previous studies reporting the adsorption capacity of *A. americana* derived materials support its evaluation as a promising precursor for low-cost bioadsorbents.

While Agave-derived materials exhibit promising adsorption performance, the impact of relatively mild physical and chemical treatments on their lignocellulosic structure and metal-binding properties is still not well understood. Unlike more aggressive modification methods involving carbonization, high temperatures, or concentrated chemical reagents, thermal, ultrasonic, and moderate alkaline treatments can improve the accessibility of oxygen-containing functional groups and modify the distribution of adsorption sites while preserving much of the original fibrous structure. A comparative evaluation of these treatments is therefore essential to understand how changes in surface chemistry and functional-group

Table 1. Preparation conditions of the biomaterials derived from *Agave americana* leaf residues.

Biomaterial	Treatment	Experimental conditions
BN	Untreated	Washed, air-dried, ground, and sieved fibers
BT	Thermal	Autoclave treatment at 120 °C for 120 min
BU	Ultrasound	Ultrasound treatment at 70 kHz for 60 min using alternating cycles of 1 min treatment and 1 min rest
BQ	Alkaline	Immersion in 1 M NaOH at 25 °C for 6 h, followed by washing with deionized water until neutral pH

accessibility influence metal adsorption.

This study evaluated untreated and mildly treated *A. americana* leaf fibers for the removal of Fe(III) and Pb(II) from aqueous solutions. A factorial design combined with adsorption isotherm analysis was used to identify the most suitable biomaterial and operating conditions for each metal. The novelty of this work lies in the systematic comparison of four biomaterials derived from the same lignocellulosic residue under identical experimental conditions.

2 Material and methods

2.1 Bioadsorbents preparation

Mature *A. americana* leaves were collected in Nombre de Dios, Durango, Mexico (23°50'12" N, 104°13'50" W), during January and February 2023. The plants were approximately 12 years old. After collection, the leaves were washed to remove surface impurities, mechanically shredded, and air-dried at room temperature for 10 days. The dried material was then cut into approximately 2-cm pieces and used to prepare four biomaterials: untreated fibers (BN), thermally treated fibers (BT), ultrasound-treated fibers (BU), and alkali-treated fibers (BQ). The treatment conditions are summarized in Table 1.

After treatment, all materials were air-dried, ground, and sieved to obtain particle sizes of 250 and 420 μm. The resulting biomaterials were stored in sealed polyethylene bags at room temperature and protected from light until use.

Thermal treatment was carried out according to Contreras-Hernández *et al*. (2018). For the alkaline treatment, the fibers were immersed in 1 M NaOH at 25 °C for 6 h and subsequently washed with deionized water until neutral pH, following Velazquez-Jimenez *et al*. (2013). The ultrasound-treated biomaterial (BU) was prepared using a BRANSON 250 probe sonicator operating at 70 kHz. The treatment consisted of alternating cycles of 1 min of ultrasound exposure and 1 min of rest, for a total processing time of 60 min.

2.2 Characterization: infrared spectroscopy

The chemical structure of the bioadsorbents was characterized by Fourier-transform infrared spectroscopy (FT-IR) using a Bruker Tensor 37 spectrometer (Ettlingen, Germany). Measurements were performed in attenuated total reflectance (ATR) mode. Each sample was pressed uniformly against a diamond crystal using a spring-loaded anvil. Spectra were recorded in triplicate, averaging 32 scans over a wavenumber range of 500–4000 cm^{-1}.

2.3 Preparation of solutions

A 1000 $mg{\cdot}L^{-1}$ Fe(III) stock solution was prepared from iron(III) chloride hexahydrate ($FeCl_3{\cdot}6H_2O$, Jalmek®), whereas a 1000 $mg{\cdot}L^{-1}$ Pb(II) stock solution was prepared from lead(II) nitrate [$Pb(NO_3)_2$, Sigma-Aldrich®]. Stock concentrations were calculated on a metal-ion basis. Working solutions were prepared by dilution with deionized water according to the concentration ranges required for each experimental stage.

Solutions of 0.1 M NaOH and 0.1 M HCl were used for pH adjustment. NaOH was added dropwise under continuous agitation to minimize localized increases in pH and the possible formation of insoluble iron species.

An initial concentration of 5 $mg{\cdot}L^{-1}$ was used in the factorial-design experiments. For equilibrium-isotherm studies, Fe(III) concentrations ranged from 10 to 60 $mg{\cdot}L^{-1}$, whereas Pb(II) concentrations ranged from 3 to 350 $mg{\cdot}L^{-1}$.

2.4 Preliminary experimental trials

Before conducting the factorial design, repeated preliminary experiments were performed to establish suitable operating ranges for metal concentration, initial pH, and contact time. These trials were particularly important for the iron system because visible precipitation occurred when the iron concentration exceeded 60 $mg{\cdot}L^{-1}$ or when NaOH was added during pH adjustment. Therefore, iron concentrations above 60 $mg{\cdot}L^{-1}$ were excluded from the equilibrium experiments, and pH adjustment was performed gradually under continuous stirring. Control solutions without bioadsorbent were evaluated during the preliminary trials under the same initial metal concentration, pH, agitation, temperature, contact time, separation, and analytical conditions used in the adsorption experiments. These controls

were used to monitor metal stability in the aqueous phase and to distinguish adsorption-related removal from losses associated with precipitation or the experimental procedure. Based on the preliminary results, contact times of 120 min for total iron and 20 min for Pb(II) were selected for the factorial bioadsorbent-screening experiments.

2.5 Batch adsorption experiments and factorial design

A full factorial design was employed to evaluate the effects of biomaterial type, initial pH, and particle size on metal removal. The evaluated factors were biomaterial type at four levels (BN, BT, BU, and BQ), initial pH at two levels (4 and 5), and particle size at two levels (250 and 420 μm), resulting in a 4 × 2 × 2 factorial arrangement. Each of the 16 treatment combinations was evaluated in duplicate for each metal, resulting in 32 experiments for total iron and 32 for Pb(II), for a total of 64 experimental runs. The residual metal concentration in the liquid phase, expressed as mg·L^{-1}, was used as the response variable.

Each experiment was conducted in a 15 mL flask containing 10 mL of a single-metal solution and 0.02 g of biomaterial, corresponding to an adsorbent dosage of 2 g·L^{-1}. The initial metal concentration was fixed at 5 mg·L^{-1}. The suspensions were agitated at 240 rpm using an orbital shaker (IKA® KS 130 Basic) at room temperature. Temperature was not externally controlled because the experiments were designed to evaluate adsorption under ambient conditions. Contact times of 120 min for Fe^{3+} and 20 min for Pb^{2+} were used according to the preliminary experiments. At the end of the established contact time, the samples were centrifuged to separate the biomaterial from the aqueous phase, and the residual metal concentration was determined by atomic absorption spectroscopy.

2.6 Analytical measurements

Residual total Fe and Pb concentrations were quantified using an atomic absorption spectrophotometer (GBC Avanta) operated in direct aspiration mode. The analytical response was calibrated using standard solutions prepared from certified 1000 mg·L^{-1} metal standards. Calibration curves were linear up to 5 mg·L^{-1}, with determination coefficients of 0.999 for total iron and 0.998 for Pb.

Samples exceeding the calibration range were diluted before analysis to ensure that all measurements remained within the validated linear interval. All measurements were conducted using the same instrumental and flame conditions applied during calibration.

2.7 Adsorption capacity and removal efficiency

The amount of metal adsorbed at a given contact time, q_t, was calculated using Eq. (1):

$$q_t = \frac{(C_0 - C_t)V}{m} \tag{1}$$

The metal removal efficiency was calculated using Eq. (2):

$$\%R = \frac{(C_0 - C_t)}{C_0} \times 100 \tag{2}$$

where C_o is the initial metal concentration in the liquid phase (mg·L^{-1}), C_t is the residual metal concentration at contact time t (mg·L^{-1}), V is the solution volume (L), and m is the dry mass of bioadsorbent (g).

Under equilibrium conditions, C_t and q_t were expressed as C_e and q_e, respectively (Santos *et al.* 2019). Metal ion concentrations after the adsorption process were determined by AAS.

2.8 Statistical analysis

The experimental data were analyzed using Minitab® software. The normality of the data was evaluated using the Anderson–Darling test. When necessary, a Box–Cox transformation was applied to improve compliance with the normality assumption. Analysis of variance (ANOVA) was used to assess the statistical significance of the main factors and their interactions when the assumptions required for parametric analysis were satisfied. When normality could not be achieved, the non-parametric Kruskal–Wallis test was applied to evaluate statistically significant differences. Statistical significance was established at a 95% confidence level ($p<0.05$). Because the biomaterials exhibited markedly different adsorption performances, the effects of initial pH and particle size were also analyzed separately for each biomaterial to netter evaluate their influence within each treatment group.

2.9 Adsorption isotherms

After identifying the optimal operating conditions and the most effective biomaterial, adsorption isotherm studies were performed using the selected adsorbent. Solutions of Pb^{2+} and Fe^{3+} were prepared at six different initial concentrations using $Pb(NO_3)_2$ and $FeCl_3{\cdot}6H_2O$, respectively. The previously optimized pH and particle size conditions were applied in all trials.

Fe(III) containing solutions were evaluated at initial concentrations of 10, 15, 30, 45, and 60 mg·L^{-1}, with samples collected after 15, 30, 45, 60, and 120 min. Pb(II) solutions were evaluated at initial concentrations of 3, 5, 30, 75, 175, and 350 mg·L^{-1}, with samples collected after 5, 10, 15, 20, and 30 min.

Each experiment was performed in duplicate in a 15 mL flask containing 10 mL of metal solution and 0.02 g of the selected biomaterial. The suspensions were agitated at 240 rpm at room temperature (IKA® KS 130 Basic). The optimized conditions were pH 4 and a particle size of 250 μm for total iron removal using BN, and pH 5 and 250 μm for Pb(II) removal using BQ.

At each sampling time, 7 mL aliquots were centrifuged using a HERMLE Z206A centrifuge at 6000 rpm for 5 min and subsequently filtered to remove suspended biomaterial particles. Residual metal concentrations were quantified by atomic absorption spectroscopy (AAS).

Based on the contact-time results, data obtained after 60 min for total iron and after 10 min for Pb(II) were used to construct the adsorption isotherms.

The equilibrium adsorption capacity (q_e) was calculated using the mass balance expression provided in Eq. (1).

To describe the adsorption behavior, the experimental data were fitted to the Langmuir and Freundlich isotherm models (Awual *et al*. 2018; Benzaoui *et al*. 2018). The Langmuir isotherm, expressed in Eq. (3), assumes adsorption occurs on a homogeneous surface with a finite number of identical sites, leading to monolayer coverage. According to this model, once a site is occupied, no further adsorption can occur at that location (Langmuir, 1918). Mathematically, the isotherm is represented as follows:

$$q_e = \frac{Q_{\max} k_L C_e}{1 + k_L C_e} \tag{3}$$

The Langmuir equilibrium constant, K_L (L·mg^{-1}), provides an estimate of the affinity between the adsorbent and the adsorbate and is related to the free energy of the adsorption process. At equilibrium, C_e (mg·L^{-1}) corresponds to the residual metal concentration in the liquid phase, while Q_{max} (mg·g^{-1}) represents the theoretical maximum adsorption capacity per unit mass of adsorbent.

In contrast, the Freundlich isotherm (Eq. 4) describes adsorption on energetically heterogeneous surfaces and assumes the formation of multilayer coverage. This empirical model accounts for the non-uniform distribution of adsorption sites and possible interactions among adsorbed species (Freundlich, 1906).

$$q_e = K_F C_e^{\frac{1}{n}} \tag{4}$$

In the Freundlich model, K_F and n are empirical constants associated with adsorption capacity and adsorption intensity (or surface heterogeneity), respectively.

Adsorption isotherms were fitted using OriginLab 2024® software. Experimental data were fitted to both the Langmuir and Freundlich equations using the nonlinear curve-fitting function. The goodness of fit of each model was comparatively evaluated to determine which more accurately described the adsorption behavior. From the best-fitting model, the corresponding isotherm parameters were obtained.

3 Results and discussions

3.1 FT-IR Characterization of adsorbent materials

Fourier-transform infrared (FT-IR) spectroscopy was used to characterize the surface chemistry of the prepared biomaterials and identify the functional groups potentially involved in heavy metal adsorption. Figure 1 presents the spectra of the four biomaterials derived from *A. americana* residues (BN, BT, BU, and BQ). Overall, the spectra are consistent with those typically reported for lignocellulosic materials, indicating that the main structural components of the agave fibers were preserved after the different treatments.

In the region between 4000 and 3000 cm^{-1}, all biomaterials exhibited a broad absorption band centered at approximately 3400 cm^{-1}. This band is attributed to O–H stretching vibrations associated with hydroxyl groups present in cellulose, hemicellulose, and lignin, as well as physically adsorbed water. Its broad profile is consistent with intra- and intermolecular hydrogen bonding within the lignocellulosic matrix (Luzardo *et al*. 2015; Hospodarova *et al*. 2018). Hospodarova *et al*. (2018) similarly assigned the broad band near 3331 cm^{-1} to hydroxyl-group stretching and hydrogen-bond interactions in cellulosic fibers.

A well-defined absorption band was also observed in the 2900–2950 cm^{-1} region. This signal was attributed to the stretching vibrations of aliphatic C–H bonds in methyl (–CH_3) and methylene (–CH_2) groups, which are characteristic of the aliphatic backbone of cellulose, hemicellulose, and lignin (Contreras-Hernández *et al*. 2018). This assignment is consistent with the band near 2894 cm^{-1} reported for the C–H stretching vibrations of the hydrocarbon constituents of polysaccharides (Hospodarova *et al*. 2018).

The absorption band located near 1730 cm^{-1} was assigned to the C=O stretching vibrations of unconjugated carbonyl groups. In lignocellulosic biomass, this signal is commonly associated with acetyl and ester groups in hemicellulose, as well as with carboxylic acids, aldehydes, ketones, lignin structures, and surface extractives (Velazquez-Jimenez *et al*. 2013; Kaur *et al*. 2024). Differences in band shape or relative intensity among BN, BT, BU, and

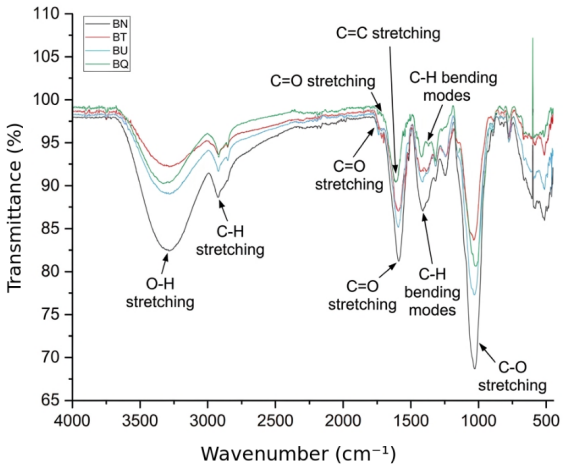

Figure 1. FT-IR Spectra of biomaterials BN, BT, BU, and BQ biomaterials derived from Agave americana leaf residues over the wavenumber range of 4000–500 cm^{-1}.

BQ may reflect changes in the accessibility or relative contribution of carbonyl-containing components after treatment. However, these observations should be interpreted qualitatively rather than direct evidence of compositional changes.

The region between approximately 1650 and 1600 cm^{-1} may contain overlapping contributions from the bending vibrations of physically adsorbed water, conjugated carbonyl groups, and aromatic C=C vibrations associated with lignin. Therefore, this region should not be assigned exclusively to a single functional group. Hospodarova *et al.* (2018) related a band near 1633 cm^{-1} to water absorbed by cellulose, whereas lignocellulosic studies have also associated signals in this region with aromatic structures in lignin. Together, these functional groups provide potential active sites for metal ion binding, supporting the suitability of these materials for adsorption applications.

Several absorption bands were detected in the 1400–1200 cm^{-1} region, which are generally associated with C–O stretching vibrations in carboxylate groups (COO^{-}), alcohols (C–OH), and ether linkages (C–O–C) (Grams 2022). Additional bands between 1250 and 1050 cm^{-1} were assigned to C–O stretching vibrations of alcohols and ethers, further confirming the presence of cellulose and related biopolymers in all samples. This region has been consistently reported for cellulosic fibers, where bands near 1027 cm^{-1} have been linked to stretching and bending vibrations of $–CH_2$, –OH, and C–O bonds in cellulose (Hospodarova *et al.* 2018). Given the overlapping nature of these vibrations, however, this region should be interpreted as reflecting the overall carbohydrate framework rather than allowing a precise discrimination between individual polysaccharide components.

In the lower wavenumber range (800–600 cm^{-1}), weak absorption bands were observed that may be attributed to Si–O vibrations, possibly arising from trace silica or residual inorganic components within the biomass. Silica extracted from plant residues has been reported to display Si–O bending and stretching vibrations in a comparable region, near 800 and 1050 cm^{-1} (silica extraction from plant biomass studies). Although these signals are of low intensity in the present spectra, these bands may indicate minor mineral fractions in the biomaterial, consistent with previous reports of trace silica content in agricultural and agave-derived residues (Kaur *et al.* 2024). It should be noted that, without complementary elemental analysis (e.g., EDS or XRF), this assignment remains tentative and should be regarded as a qualitative indication rather than confirmed evidence of silica content.

Among the samples, BN exhibited slightly higher peak intensities in several regions, particularly in the O–H and C–O stretching bands, which may indicate a greater abundance of accessible hydroxyl groups or retained moisture compared to the treated materials. In contrast, BQ and BT displayed nearly overlapping spectral profiles, pointing to a high degree of structural similarity, with comparable functional group distributions.

This similarity may be associated with structural modifications linked to partial delignification, which can increase the exposure of cellulose-related functional groups and enhance their chemical accessibility (Chakraborty *et al.* 2024). The BU material presented a slightly more pronounced absorption around 2900 cm^{-1}, suggesting a relatively higher contribution of C–H bonds or subtle changes in the relative proportion of cellulose and lignin components; this behavior is consistent with the disruptive effect of acoustic cavitation during ultrasonic treatment, where localized high shear forces can alter the lignocellulosic matrix (Contreras-Hernández *et al.* 2018). Nonetheless, since FT-IR provides only qualitative information on relative band intensities, these observations should be regarded as indicative trends rather than quantitative measures of compositional change, and would benefit from confirmation through complementary techniques such as TGA or elemental analysis.

From an adsorption standpoint, the presence of COOH, OH, and C=O groups identified across all four materials is relevant, as these functional groups can act as active binding sites for Fe^{3+} and Pb^{2+} ions through electrostatic attraction and coordination interactions involving electron-rich oxygen atoms (Zadehahmadi *et al.* 2023). This interpretation is supported by previous studies on Agave-derived lignocellulosic materials, where FT-IR characterization identified hydroxyl, carboxyl, and carbonyl functional groups enabling the biosorption of heavy metals from aqueous

solutions (Flores-Trujillo *et al*. 2021). Similarly, agave bagasse functionalized for water remediation exhibited C–O, C=O, –OH, and O–C=O surface groups consistent with those observed in the present study (Gómez-Navarro *et al*. 2023). In a related system, functionalized cellulose fibers obtained from *A. americana* (cabuya) residues achieved a Hg(II) removal efficiency above 92%, with FT-IR confirming the involvement of hydroxyl and carbonyl surface groups in the adsorption mechanism (Sánchez-Moreno *et al*. 2025). The relevance of these oxygen-containing groups is not restricted to Agave-derived materials or to a single metal ion: comparable FT-IR profiles, dominated by hydroxyl, carbonyl, hydrocarbon, and aromatic functionalities, have been reported for other lignocellulosic bioadsorbents used in the removal of Cr(VI), including artichoke (*Cynara cardunculus* L.) (Diaz-Rodriguez *et al*. 2025) and Luffa cylindrica fibers (Moreno-Rubio *et al*. 2025), in both cases linking these functional groups directly to the metal-removal mechanism. Collectively, these studies support the interpretation that the functional groups identified in BN, BT, BU, and BQ are compatible with an active role in Fe^{3+} and Pb^{2+} adsorption. However, direct confirmation would require complementary evidence, such as FT-IR spectra before and after adsorption to detect band shifts or intensity changes associated with metal binding.

3.2 *Bioadsorbent selection*

3.2.1 *Variance analysis*

Normality tests indicated that the adsorption data for both iron and lead were consistent with a normal distribution for each biomaterial. In all cases, p-values exceeded 0.05, meaning that the null hypothesis of normality could not be rejected. These results support the use of parametric statistical methods for further analysis (Figure 2).

For Fe^{3+} adsorption, BN and BT exhibited relatively high p-values (0.790 and 0.275, respectively) along with low standard deviations (Figure 2a and 2b), indicating more stable and reproducible adsorption performance under the evaluated conditions. This consistency may be attributed to the structural effects of the applied treatments. Thermal and physical modifications can promote a more uniform distribution of active sites on the biomaterial surface, potentially facilitating more homogeneous iron uptake (Thakur *et al*. 2020).

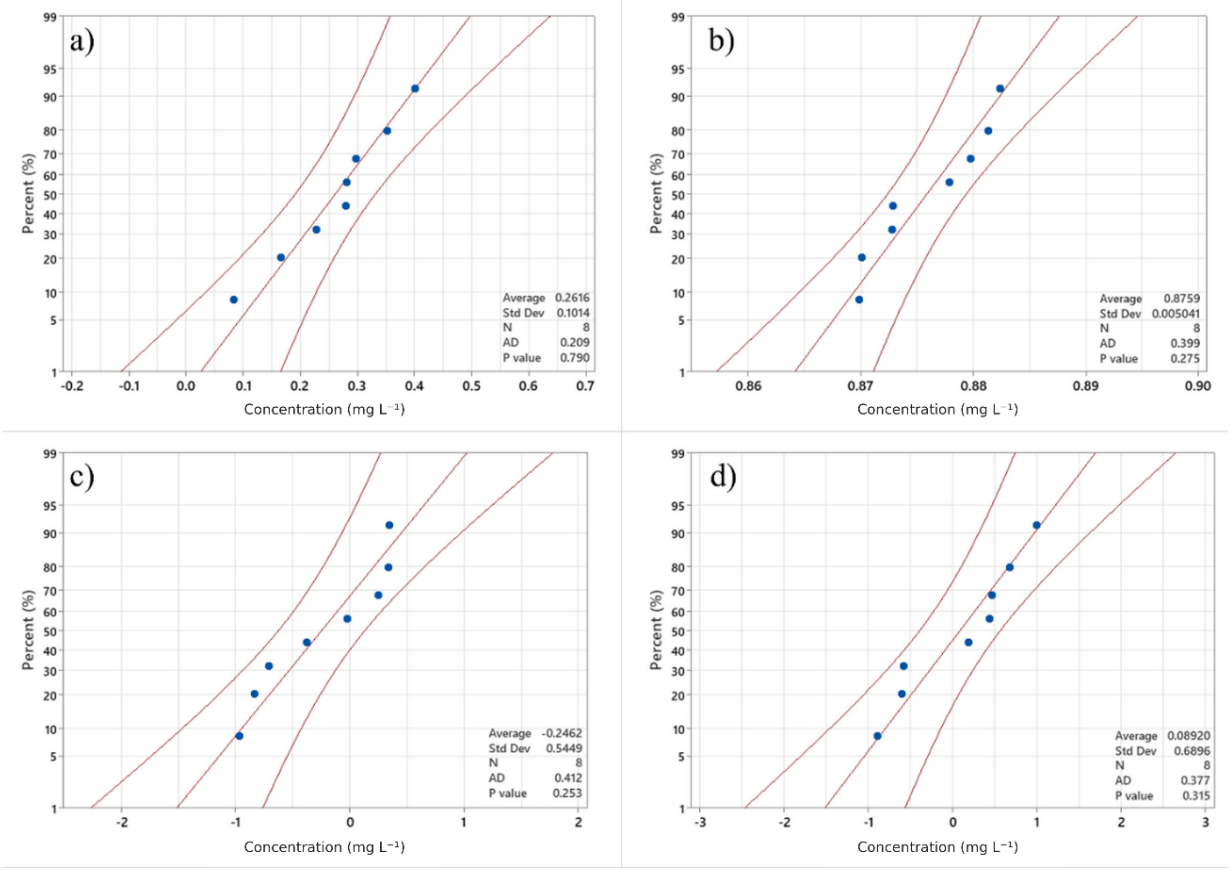

Figure 2. Normal probability plot of the Fe^{3+} adsorption process with the different Agave waste biomaterials, p=0.05, Anderson-Darling (AD) statistic, a) BN; b) BT, c) BU and d) BQ.

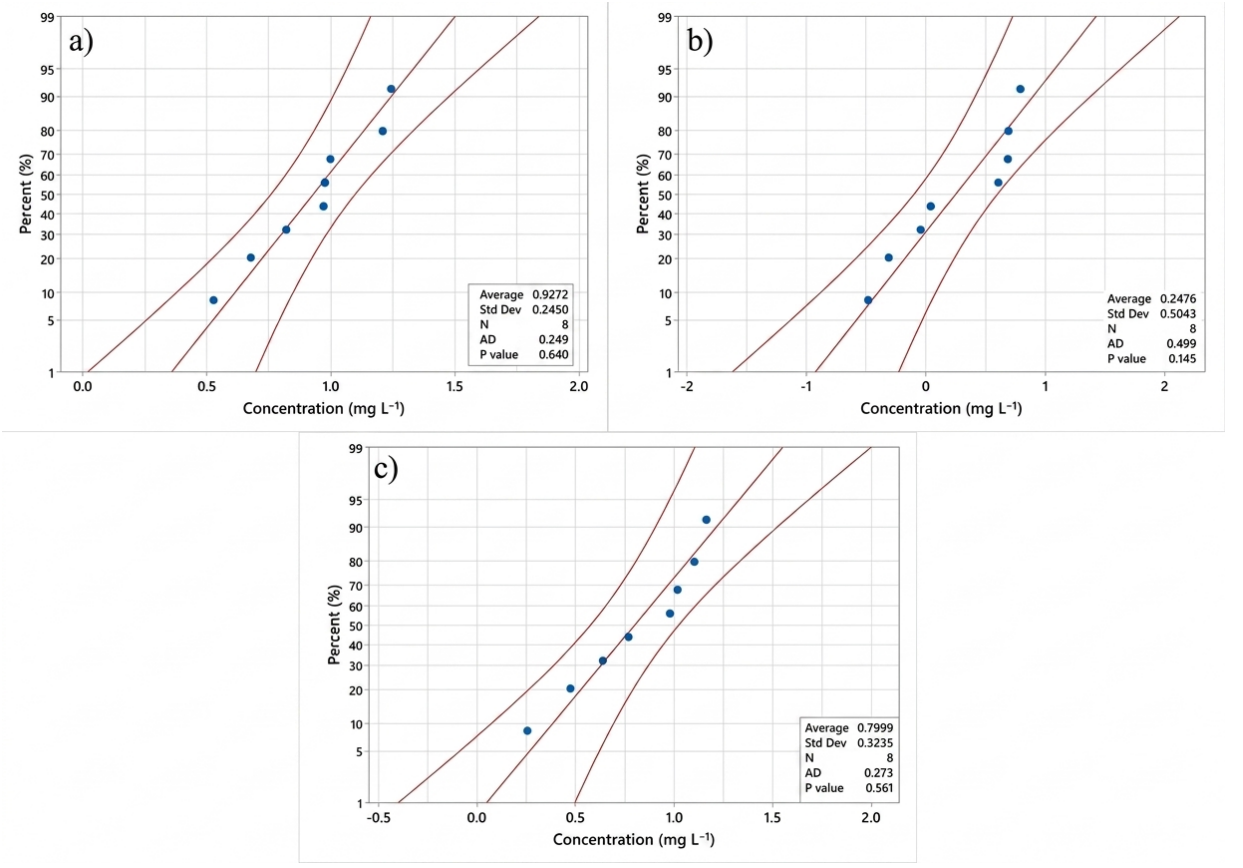

Figure 3. Standard probability plot of the Pb^{2+} adsorption process with the different Agave waste biomaterials, p=0.05, Anderson-Darling (AD) statistic, a) BN; b) BT and c) BU.

Although BU and BQ also showed distributions close to normality, both presented higher standard deviations (0.5449 and 0.6896, respectively; Figure 2c and 2d), reflecting greater variability in Fe^{3+} adsorption. This dispersion suggests that the treatments applied to these materials may have produced a less uniform surface or altered the distribution and accessibility of functional groups (Yadav *et al*. 2024). Such heterogeneity may directly influence adsorption performance, leading to less consistent metal uptake. From a practical perspective, these materials may benefit from further optimization to improve surface homogeneity and adsorption reproducibility.

For Pb^{2+} adsorption, probability plots for BN, BT, and BU yielded p-values and Anderson–Darling (AD) statistics consistent with normal data distribution (Figure 3). In the case of BN, the mean residual concentration was 0.9272 mg·L^{-1} with a standard deviation of 0.2450, values comparable to those obtained for BU (Figure 3a and 3c). These results indicate moderate variability in adsorption capacity, which may be attributed to the natural abundance of functional groups such as –OH and –COOH on the untreated or physically treated surfaces. These functional groups are known to promote Pb^{2+} adsorption even in the absence of chemical modification (Thakur *et al*. 2020).

In contrast, BT exhibited lower Pb^{2+} adsorption capacity and greater variability compared to BN. Thermal treatment can modify lignocellulosic structures, particularly by affecting hydroxyl groups (–OH), which may result in increased surface heterogeneity and reduced availability of effective binding sites for lead ions (Nighojkar *et al*. 2023). This structural alteration could explain the comparatively weaker performance observed for BT.

Notably, BQ achieved complete (100%) removal of Pb^{2+} under the evaluated conditions and, for this reason, was not included in the probability plot. This outstanding performance is consistent with previous findings indicating that chemical treatments can significantly enhance adsorption capacity by increasing the exposure or reactivity of functional groups involved in metal binding (de Quadros Melo *et al*. 2016; Nighojkar *et al*. 2023; Yadav *et al*. 2024).

Materials exhibiting low standard deviations and normally distributed adsorption data are generally associated with greater structural homogeneity and more predictable adsorption performance (Tejada-Tovar *et al*. 2019; Thakur *et al*. 2020; Yadav *et al*. 2024). In practical terms, reduced variability in adsorption data suggests greater structural consistency and more predictable performance. These findings

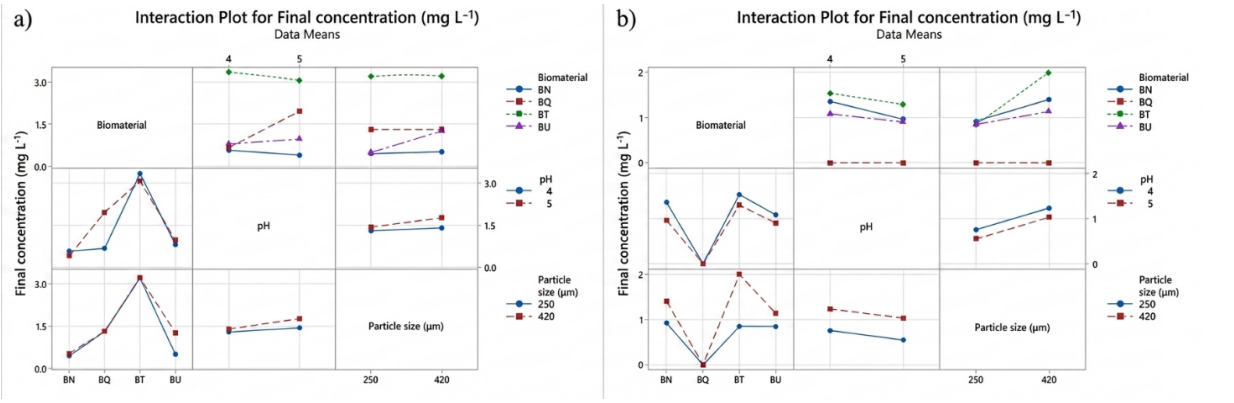

Figure 4. Interaction of biomaterial, pH and particle size in the final concentration of metals after the adsorption process using biomaterials derived from agave residues: a) Fe^{3+} and b) Pb^{2+}.

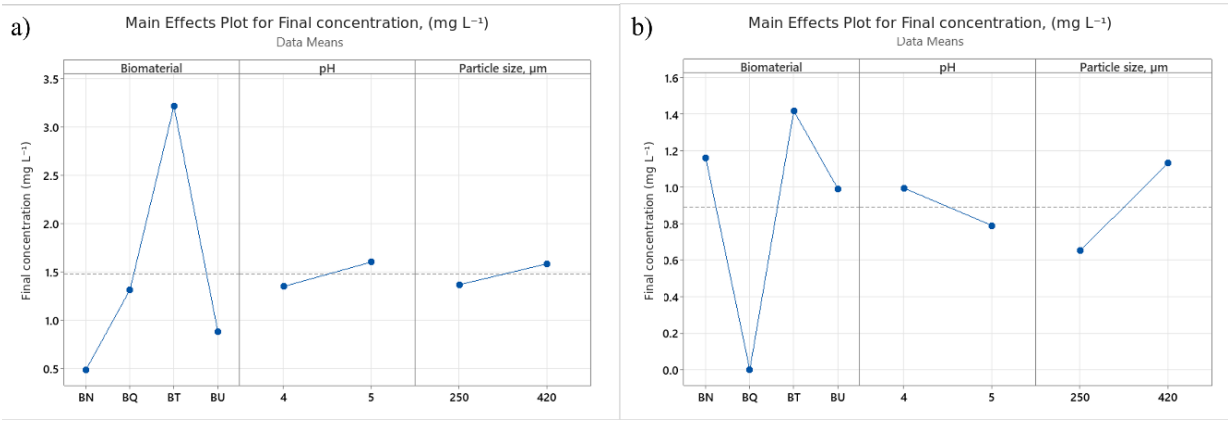

Figure 5. Main effects of biomaterial, pH, and particle size on the final concentration of metals after the adsorption process using biomaterials derived from agave residues: a) Fe^{3+} and b) Pb^{2+}.

further support the potential of *Agave*-derived biomaterials as effective adsorbents, particularly those demonstrating stable and reproducible adsorption behavior.

3.2.2 Main effects and interaction of parameters

The main effects and interaction plots provide a visual representation of how the final metal concentration responds to variations in biomaterial type, pH, and particle size. They also allow assessment of whether these factors act independently or synergistically.

For Fe^{3+} removal (Figures 4a and 5a), the adjusted means indicate that BT was the least effective material, yielding higher residual iron concentrations relative to the other biomaterials. In contrast, BN achieved the greatest reduction in Fe^{3+} concentration, reaching an average final value close to 0.5 mg·L^{-1}. The most favorable conditions for iron adsorption were observed at pH 4 and a particle size of 250 μm, which correspond to the optimal parameters identified in the experimental design.

The superior performance observed at lower pH can be attributed to a reduced competition between metal ions and hydroxide species in solution, which promotes stronger interaction between Fe^{3+} and the active sites of the adsorbent surface (Arias and Sen 2009; Febrianto *et al*. 2009). Additionally, decreasing particle size increases the available surface area, thereby improving contact between the biomaterial and the metal ions and enhancing adsorption efficiency (Foo and Hameed 2010).

Analysis of the adjusted means and interaction plots for Pb^{2+} adsorption (Figures 4b and 5b) shows that BN, BT, and BU exhibited comparable removal performance under the evaluated conditions. However, a markedly different behavior was observed for BQ (Figure 5b), which achieved complete removal of lead ions from the tested solutions.

The adsorption process was moderately enhanced at an initial pH of 5 and more strongly favored when smaller particle sizes (250 μm) were used (Figure 4b). The reduction in particle size increases the available surface area and, consequently, the number of accessible sorption sites, facilitating greater Pb^{2+} uptake (Febrianto *et al*. 2009; Foo & Hameed, 2010).

The slight improvement at pH 5 may be associated with more favorable electrostatic interactions between the biomaterial surface and lead ions under these conditions.

Overall, BQ was identified as the most effective biomaterial for Pb^{2+} adsorption. Within the evaluated experimental range, variations in pH and particle size had little influence on its performance because complete removal was achieved under all tested conditions (Figures 4b and 5b).

Among the variables evaluated, the type of biomaterial clearly emerged as the dominant factor influencing adsorption performance. Although pH and particle size contributed to process optimization, their effects were secondary compared to the intrinsic properties of the adsorbent. For Fe^{3+} removal, BN demonstrated the highest efficiency, reaching 82.86% removal at pH 4 with a particle size of 250 μm. Notably, variations in pH and particle size did not produce substantial changes in its performance, suggesting that the material itself governs the adsorption behavior. In the case of Pb^{2+}, BQ proved to be the most effective adsorbent, achieving complete (100%) removal under all tested conditions, with optimal performance observed at pH 5 and a particle size of 250 μm.

3.2.3 Adsorption isotherms

To establish an appropriate contact time for constructing adsorption isotherms, preliminary kinetic experiments were conducted. Fe^{3+} adsorption was evaluated using BN, while Pb^{2+} adsorption was assessed using BQ, each at different initial metal concentrations (Tables 2 and 3).

Table 2. Time-dependent adsorption of Fe^{3+} at different initial concentrations for equilibrium time determination by the BN biomaterial.

	C_0 (mg·L^{-1})	Time (min)	Ce (mg·L^{-1})	q_t (mg·g^{-1})	Removal (%)
Fe^{3+}	10	0	10±0.00	0±0.00	0.00±0.00
		15	0.157±0.04	3.961±0.04	98.05±0.04
		30	0.078±0.01	4.001±0.01	99.03±0.01
		45	0.389±0.18	3.845±0.18	95.18±0.18
		60	0.376±0.20	3.851±0.20	95.34±0.20
		120	0.935±0.06	3.572±0.06	88.43±0.06
	15	0	15±0.00	0±0.00	0.00±0.00
		15	0.08±0.05	7.71±0.05	99.48±0.05
		30	0.295±0.01	7.602±0.01	98.10±0.01
		45	0.335±0.06	7.582±0.06	97.84±0.06
		60	0.695±0.08	7.402±0.08	95.52±0.08
		120	1.32±0.11	7.09±0.11	91.48±0.11
	30	0	30±0.00	0±0.00	0.00±0.00
		15	0.95±0.01	14.013±0.01	96.72±0.01
		30	1.34±0.17	13.818±0.17	95.38±0.17
		45	2.00±0.002	13.485±0.002	93.07±0.002
		60	2.09±0.02	13.443±0.02	92.79±0.02
		120	2.845±0.05	13.066±0.05	90.18±0.05
	45	0	45±0.00	0±0.00	0.00±0.00
		15	0.40±0.02	22.63±0.02	99.12±0.02
		30	1.94±0.09	21.86±0.09	95.75±0.09
		45	3.15±0.03	21.26±0.03	93.10±0.03
		60	4.62±0.24	20.52±0.24	89.88±0.24
		120	11.43±0.75	17.12±0.75	74.97±0.75
	60	0	60±0.00	0±0.00	0.00±0.00
		15	0.13±0.04	31.29±0.04	99.79±0.04
		30	3.57±0.33	29.57±0.33	94.31±0.33
		45	6.08±0.05	28.31±0.05	90.30±0.05
		60	6.99±0.94	27.86±0.94	88.85±0.94
		120	1.38±0.05	30.66±0.05	97.81±0.05

Table 3. Time-dependent adsorption of Pb^{2+} at different initial concentrations for equilibrium time determination by the BQ biomaterial.

	C_0 (mg·L^{-1})	Time (min)	Ce (mg·L^{-1})	q_t (mg·g^{-1})	Removal (%)
Pb^{2+}	3	0	3.00±0.00	0.00±0.00	0.00±0.00
		5	0.652±0.18	0.91±0.18	73.67±0.18
		10	0.136±0.05	1.17±0.05	94.53±0.05
		15	0.148±0.03	1.16±0.03	94.02±0.03
		20	0.118±0.00	1.18±0.00	95.23±0.00
		30	0.084±0.03	1.20±0.03	96.63±0.03
	5	0	5.00±0.00	0.00±0.00	0.00±0.00
		5	1.760±0.37	2.27±0.37	72.05±0.37
		10	0.722±0.13	2.79±0.13	88.54±0.13
		15	0.363±0.04	2.97±0.04	94.24±0.04
		20	0.267±0.10	3.02±0.10	95.76±0.10
		30	0.539±0.41	2.88±0.41	91.45±0.41
	30	0	30±0.23	0.00±0.00	0.00v0.00
		5	13.524±1.14	8.07±1.14	54.42±1.14
		10	4.956±0.49	12.36±0.49	83.30±0.49
		15	3.074±0.05	13.30±0.05	89.64±0.05
		20	2.08±0.11	13.80±0.11	92.99±0.11
		30	1.938±0.57	13.87±0.57	93.47±0.57
	75	0	75.06±0.04	0.00±0.00	0.00±0.00
		5	28.52±2.79	23.27±2.79	62.00±2.79
		10	16.19±1.33	29.43±1.33	78.43±1.33
		15	13.38±1.79	30.84±1.79	82.17±1.79
		20	10.40±0.31	32.33±0.31	86.14±0.31
		30	7.69±0.11	33.68±0.11	89.75±0.11
	175	0	175.1±0.034	0.00±0.00	0.00±0.00
		5	76.12±1.06	48.49±1.06	56.02±1.06
		10	69.96±4.48	51.57±4.48	59.59±4.48
		15	76.15±1.52	48.48±1.52	56.01±1.52
		20	80.12±1.31	46.49±1.31	53.71±1.31
		30	75.96±2.89	48.57±2.89	56.12±2.89
	350	0	350.4±0.009	0.00±0.00	0.00±0.00
		5	203.29±1.85	67.05±1.85	39.75±1.85
		10	228.08±1.43	54.66±1.43	32.40±1.43
		15	248.96±2.48	44.22±2.48	26.21±2.48
		20	242.21±2.18	47.60±2.18	28.21±2.18
		30	247.37±2.48	45.01±2.48	26.68±2.48

For Fe^{3+} adsorption onto BN, high removal efficiencies were observed even at short contact times across all tested concentrations. In most cases, removal exceeded 95% within the first 15 minutes. As contact time increased, a slight decrease in removal efficiency was noted, particularly at higher initial concentrations. This trend may be related to partial site saturation and subsequent redistribution of Fe^{3+} ions between the solid and liquid phases as the system approaches equilibrium (Foo and Hameed 2010). After approximately 60 minutes, adsorption values stabilized, indicating that equilibrium had been reasonably attained. Based on this behavior, a contact time of 60 minutes was selected for the construction of the Fe^{3+} adsorption isotherms (Table 2).

The BN biomaterial demonstrated strong affinity for Fe^{3+}, particularly during the initial stages of contact, where removal efficiencies approached 100%. This rapid uptake suggests a high availability of accessible active sites on the surface. However, as contact time increased, especially at higher initial metal concentrations, a gradual decline in removal efficiency was observed. The system appeared to stabilize after approximately 60 minutes, indicating that adsorption desorption dynamics had reached equilibrium under the evaluated conditions.

For Pb^{2+} adsorption using the BQ biomaterial, a similarly rapid uptake was observed at low to moderate initial concentrations (3–75 mg·L^{-1}).

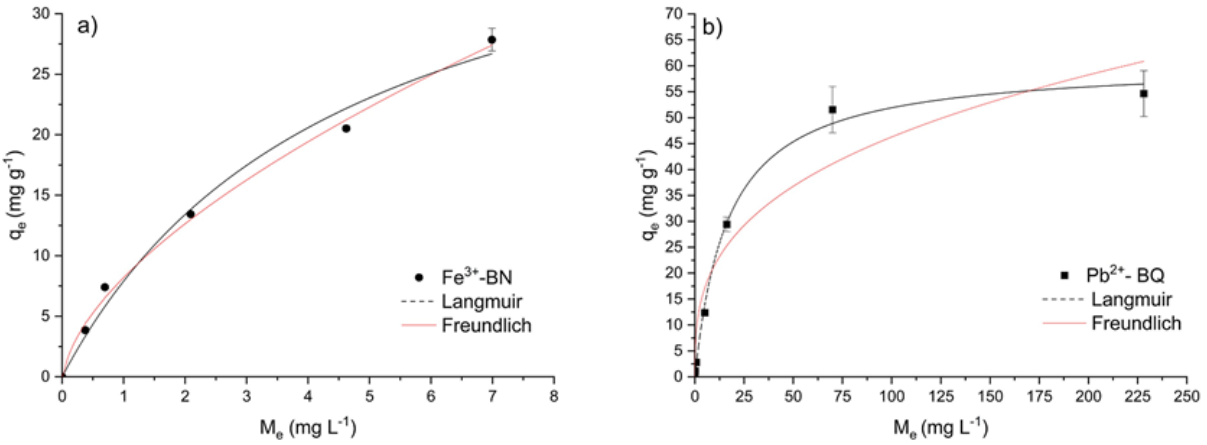

Figure 6. Fits of the isotherms models to the experimental data fits, a) Fe^{3+}: pH 4, 60 min, 240 rpm, 25 °C. b) Pb^{2+}: pH 5, 10 min, 240 rpm, 25°C.

Table 4. Comparison of Langmuir and Freundlich isotherm parameters for Fe^{3+} and Pb^{2+} adsorption, including goodness-of-fit (R^2) and Akaike information criterion (AIC).

Model	Parameters	Pb^{2+}	Fe^{3+}
Langmuir	Q_{max}, mg/g	**60.69**	**44.28**
	K_L, L/mg	0.06	0.22
	R^2	1.00	0.99
	AIC	18.46	18.96
Freundlich	K_F, L/mg	10.03	8.34
	n	3.01	1.63
	R2	0.93	1.00
	AIC	38.80	11.28

In these cases, equilibrium was reached within 10–20 minutes, with removal efficiencies consistently above 90% (Table 3). Extending the contact time beyond this range produced only slight increases in adsorption capacity, suggesting that equilibrium had already been established. In contrast, at higher initial concentrations (175 and 350 mg·L^{-1}), removal efficiency decreased significantly and showed minimal variation with time. This behavior indicates early saturation of the available adsorption sites at elevated metal loadings. Based on these findings, a contact time of 10 minutes was selected as representative of equilibrium conditions for constructing the Pb^{2+} adsorption isotherms.

The equilibrium data for Fe^{3+} adsorption onto BN showed good agreement with both the Langmuir and Freundlich isotherm models, with coefficients of determination (R^2) of 0.987 and 0.996, respectively (Figure 6a and Table 4). While both models adequately represented the experimental results, the Freundlich model provided a better overall fit, as indicated by its lower Akaike Information Criterion (AIC = 11.28) compared to the Langmuir model (AIC = 18.96). This result indicates that the Freundlich equation provides a more appropriate description of the equilibrium data while maintaining an appropriate balance between model fit and complexity.

The better performance of the Freundlich model indicates that Fe^{3+} adsorption on BN likely occurs over a heterogeneous surface, characterized by a non-uniform distribution of active sites. The Freundlich constant (K_F = 8.34 L mg^{-1}) further reflects the strong affinity of BN for Fe^{3+} ions (Table 4). In contrast to the Langmuir model, which assumes monolayer adsorption on a homogeneous surface, the Freundlich model accounts for variations in adsorption energy and site heterogeneity. This behavior suggests competition among Fe^{3+} ions for adsorption sites and the possible formation of multilayer adsorption under the evaluated conditions (Santos *et al*. 2019; Vázquez-Sánchez *et al*. 2023).

According to the Freundlich model, adsorption initially occurs at the most energetically favorable sites. As these sites become progressively occupied, adsorption shifts toward sites with lower binding energies, resulting in a gradual reduction in adsorption strength (Hernández-Francisco *et al*. 2020). This behavior can be attributed to the functional groups present in the BN biomaterial, particularly carboxyl and hydroxyl groups, which exhibit strong affinity for metal ions. The value of the constant *n* further supports this interpretation, indicating favorable adsorption conditions. It suggests that chemisorption predominates at the most active sites during the initial stages, followed by a greater contribution of physisorption mechanisms as site saturation occurs (Vigdorowitsch *et al*. 2021).

In contrast, Pb^{2+} adsorption onto the BQ biomaterial was more appropriately described by the Langmuir model (Figure 6b). This model showed a higher coefficient of determination (R^2 = 0.996) and a substantially lower AIC value (18.46) compared to

Table 5. Comparison of maximum adsorption capacities (Q_{max}) obtained in the present study with values reported for other Agave-derived and agro-industrial waste bioadsorbents, ordered by increasing capacity within each metal.

Adsorbent	Metal	Treatment	Q_{max} (mg·g^{-1})	Reference
Sugarcane bagasse biochar	Pb^{2+}	Pyrolysis (biochar)	12.74	(Poonam and Kumar 2018)
Raw agave bagasse		Untreated	35.60	(Velazquez-Jimenez *et al*. 2013)
A. tequilana cellulose nanofibrils/nanosheets		Cellulose isolation + microfluidization	43.55	(Hernández-Francisco *et al*. 2020)
A. americana BQ		**1 M NaOH, 6 h**	**60.69**	**Present study**
Cocoa agro-industrial waste (WCT)		Raw biosorbent	123.50	(Lavado-Meza *et al*. 2023)
Coffee agro-industrial waste (WCA)		Raw biosorbent	158.70	
Functionalized sugarcane bagasse		Concerted oxidation + deprotonation	200.30	(Ai *et al*. 2021)
Rice-husk-derived activated carbon	Fe^{3+}	Carbonization at 700°C	28.90	(Elewa *et al*. 2023)
A. americana BN		**Untreated**	**44.28**	**Present study**

the Freundlich model (R^2 = 0.928; AIC = 38.80), indicating that the Langmuir equation provides the best representation of the experimental data (Table 4). These findings suggest that Pb^{2+} adsorption takes place predominantly as a monolayer on a surface characterized by energetically homogeneous adsorption sites (Alafnan *et al*. 2021; Xie *et al*. 2020).

Although lignocellulosic biomaterials are typically characterized by heterogeneous surfaces containing a variety of functional groups (such as carboxyl, hydroxyl, and amine moieties), the present results suggest a more specific interaction pattern for Pb^{2+}. In this case, carboxyl groups may play a predominant role in binding lead ions, leading to adsorption behavior that closely follows the Langmuir model (Xie *et al*. 2020). This indicates that, despite the structural heterogeneity of the material, Pb^{2+} adsorption may occur preferentially at a relatively uniform set of active sites.

The maximum adsorption capacity (Q_{max}) predicted by the Langmuir model for Pb^{2+} was 60.69 mg·g^{-1}, reached at an equilibrium concentration (C_e) of approximately 75 mg·L^{-1}. The Langmuir affinity constant (K_L = 0.059 L·mg^{-1}), however, reflects a moderate interaction strength between Pb^{2+} ions and the biomaterial surface, suggesting that higher initial concentrations are necessary to approach site saturation.

Table 5 compares the adsorption capacities estimated for BN in the iron system and BQ for Pb(II) with values reported for other Agave-derived and agro-industrial waste biosorbents prepared using different levels of treatment complexity. For Pb(II), the capacities included in Table 5 ranged from 12.74 mg·g^{-1} for pyrolyzed sugarcane bagasse biochar (Poonam and Kumar 2018) to 200.30 mg·g^{-1} for sugarcane bagasse subjected to multistep functionalization through combined oxidation and deprotonation (Ai *et al*. 2021).

Within this comparison, the Langmuir maximum adsorption capacity of BQ was 60.69 mg·g^{-1}. This value was approximately 71% higher than the 35.60 mg·g^{-1} reported for untreated agave bagasse (Velazquez-Jimenez *et al*. 2013) and approximately 39% higher than the 43.55 mg·g^{-1} reported for cellulose nanofibrils and nanosheets obtained from *A. tequilana* Weber var. Azul through cellulose isolation and microfluidization (Hernández-Francisco *et al*. 2020). In contrast, BQ was prepared through a single alkaline-treatment step. Among the Agave-derived materials included in Table 5, BQ therefore exhibited one of the highest Pb(II) adsorption capacities using a comparatively simple preparation method.

Higher capacities were reported for coffee and cocoa agro-industrial residues, with values of 158.70 and 123.50 mg·g^{-1}, respectively (Lavado-Meza *et al*. 2023), and for multistep-functionalized sugarcane bagasse, with a capacity of 200.30 mg·g^{-1} (Ai *et al*. 2021). Therefore, BQ cannot be considered the highest-capacity agro-industrial biosorbent overall. Its principal advantage lies in the competitive adsorption performance achieved through the valorization of a locally available *A. americana* residue using a single alkaline-treatment step. Nevertheless, comparisons among studies should be interpreted cautiously because adsorption capacity is influenced by pH, initial concentration, adsorbent dosage, contact time, particle size, temperature, and the selected equilibrium model.

For the iron system, BN was better described by the Freundlich model according to its higher coefficient of determination and lower AIC value. Therefore, the Langmuir-estimated capacity of 44.28 mg·g^{-1} should be considered a comparative model parameter rather than the definitive maximum adsorption capacity of BN. This estimated value was higher than the 28.90 mg·g^{-1} reported for Fe(III) adsorption using rice-husk-derived activated carbon produced by electric-furnace carbonization at 700 °C (Elewa *et al*. 2023).

Although the experimental conditions and selected equilibrium models differed between both studies, this comparison highlights the potential of untreated BN, which did not require chemical activation or high-temperature carbonization. BN may therefore represent a comparatively simple and potentially less energy-intensive alternative for iron removal; however, confirmation of this practical advantage would require an economic and energy assessment.

The adsorption behavior observed for the iron and

Pb(II) systems differed notably. Pb(II) adsorption onto BQ was best represented by the Langmuir model, whereas the equilibrium data for the iron BN system were better described by the Freundlich model. These differences may be related to the physicochemical properties of the metal ions, including ionic size, hydration behavior, polarizability, and affinity for oxygen-containing functional groups within the lignocellulosic matrix (Febrianto *et al*. 2009). However, the adsorption capacities of both systems should not be compared as a direct measure of intrinsic metal affinity because different biomaterials, pH values, concentration ranges, and equilibrium models were used. The results instead demonstrate that the alkaline treatment favored Pb(II) uptake by BQ, whereas untreated BN was more suitable for the iron system under the evaluated conditions.

Beyond the numerical comparison of adsorption capacities, the novelty of the present work lies in the comparative evaluation of four biomaterials obtained from the same *A. americana* residue under identical experimental conditions. Rather than identifying a single universally superior material, the factorial-selection strategy demonstrated that treatment effectiveness depended on the target metal.

BQ achieved complete Pb(II) removal at the initial concentration used in the factorial screening experiments without requiring the multistep functionalization employed in some higher-capacity engineered adsorbents. This metal-specific selection of two differentiated biomaterials from a single regional waste stream distinguishes the present study from previous reports that commonly evaluate only one preparation or treatment condition. These findings further demonstrate that modification is not universally beneficial, as the untreated biomaterial performed best for iron removal, whereas alkaline treatment was specifically enhanced Pb(II) adsorption.

Conclusions

Biomaterials derived from *Agave americana* leaf residues exhibited promising performance for the removal of Fe(III) and Pb(II) from aqueous solutions. FT-IR analysis confirmed the presence of hydroxyl, carbonyl and carboxyl groups that may act as potential metal-binding sites.

Among the evaluated materials, untreated BN showed the best performance for the iron system, reaching a maximum removal efficiency of 82.86%. Its equilibrium data were better described by the Freundlich model, whereas the value of 44.28 $mg{\cdot}g^{-1}$ estimated by the Langmuir model should be considered only as a comparative parameter. For Pb(II), alkali-treated BQ achieved complete removal under the factorial-design conditions and a Langmuir maximum adsorption capacity of 60.69 $mg{\cdot}g^{-1}$, exceeding values reported for other Agave-derived materials.

These findings support the valorization of *A. americana* residues as precursors for metal-specific bioadsorbents. Nevertheless, further studies using real water, multicomponent systems, regeneration cycles, and continuous-flow conditions are required before practical application can be established.

Declaration of generative AI and AI-assisted technologies

During the revision of this manuscript, the authors used OpenAI's ChatGPT to assist with English-language editing and text organization. All AI-assisted content was critically reviewed, corrected, and verified by the authors, who assume full responsibility for the accuracy, scientific interpretation, originality, and final content of the manuscript.

Acknowledgements

Authors thank the Secretaría de Ciencia, Humanidades, Tecnología e Innovación (SECIHTI-Mexico) for grant support for postdoctoral research stays funding (Contreras-Hernández 489313).

Nomenclature

$\mathbf{C_0}$	Initial liquid phase concentrations of metals ($mg\ L^{-1}$)
$\mathbf{C_e}$	Steady state liquid phase concentrations of metals ($mg\ L^{-1}$)
$\mathbf{K_L}$	Langmuir adsorption constant related to adsorption affinity of metals on the bioadsorbents ($L\ mg^{-1}$)
$\mathbf{K_F}$	Adsorption affinity constant in Freundlich isotherm ($mg^{1-n}.L^{1-n}.g_A{}^{-1}$)
$\boldsymbol{m}$	Mass of adsorbent contained in the adsorption system (g_A)
n	Adsorption affinity constant (dimensionless)
$\mathbf{q_e}$	Amount of metals adsorbed on a unit weight of adsorbent at equilibrium ($mg\ g_A{}^{-1}$)
V	Volume of the adsorption system
t	Contact time of the adsorbent with the contaminated solution (min)
$\mathbf{Q_{max}}$	Maximum adsorption capacity ($mg\ g^{-1}$)
SSE	Sum of squares of the errors
$\mathbf{M_e}$	Chemical species equilibrium concentration ($mg\ L^{-1}$)

R	Removal percentage (%)

Abbreviations

AAS	Atomic Absorption Spectrophotometer
AIC	Akaike Information Criterion

References

Ai, S., Huang, Y., Huang, C., Yang, X., Zhu, W. and Xu, Y. (2021). Lead ion adsorption on functionalized sugarcane bagasse prepared by concerted oxidation and deprotonation. *Environmental Science and Pollution Research 28*, 2728-2740. https://doi.org/10.1007/s11356-020-10692-5

Alafnan, S., Awotunde, A., Glatz, G., Adjei, S., Alrumaih, I., & Gowida, A. (2021). Langmuir adsorption isotherm in unconventional resources: Applicability and limitations. *Journal of Petroleum Science and Engineering*, *207*, 109172. https://doi.org/10.1016/j.petrol.2021.109172

Alcázar-Medina, F. A., Núñez-Núñez, C. M., Villanueva-Fierro, I., Antileo, C., & Proal-Nájera, J. B. (2020). Removal of heavy metals present in groundwater from a northern Mexico mining community using *Agave tequilana* Weber extracts. *Revista Mexicana de Ingeniería Química*, *19*(3), 1187–1199. https://doi.org/10.24275/rmiq/Bio1047

Arias, F., & Sen, T. K. (2009). Removal of zinc metal ion (Zn^{2+}) from its aqueous solution by kaolin clay mineral: A kinetic and equilibrium study. *Colloids and Surfaces A: Physicochemical and Engineering Aspects*, *348*(1–3), 100–108. https://doi.org/10.1016/j.colsurfa.2009.06.036

Awual, Md. R., Khraisheh, M., Alharthi, N. H., Luqman, M., Islam, A., Rezaul Karim, M., … Khaleque, Md. A. (2018). Efficient detection and adsorption of cadmium (II) ions using innovative nano-composite materials. *Chemical Engineering Journal*, *343*, 118–127. https://doi.org/10.1016/j.cej.2018.02.116

Benzaoui, T., Selatnia, A., & Djabali, D. (2018). Adsorption of copper (II) ions from aqueous solution using bottom ash of expired drugs incineration. *Adsorption Science & Technology*, *36*(1–2), 114–129. https://doi.org/10.1177/0263617416685099

Chakraborty, P., Kumar, R., Chakrabortty, S., Saha, S., Chattaraj, S., Roy, S., … Jeon, B.-H. (2024). Technological advancements in the pretreatment of lignocellulosic biomass for effective valorization: A review of challenges and prospects. *Journal of Industrial and Engineering Chemistry*, *137*, 29–60. https://doi.org/10.1016/j.jiec.2024.03.025

Contreras-Hernández, M. G., Ochoa-Martínez, L. A., Rutiaga-Quiñones, J. G., Rocha-Guzmán, N. E., Lara-Ceniceros, T. E., Contreras-Esquivel, J. C., … Rutiaga-Quiñones, O. M. (2018). Effect of ultrasound pre-treatment on the physicochemical composition of Agave durangensis leaves and potential enzyme production. *Bioresource Technology*, *249*, 439–446. https://doi.org/10.1016/j.biortech.2017.10.009

de Quadros Melo, D., de Oliveira Sousa Neto, V., de Freitas Barros, F. C., Raulino, G. S. C., Vidal, C. B., & do Nascimento, R. F. (2016). Chemical modifications of lignocellulosic materials and their application for removal of cations and anions from aqueous solutions. *Journal of Applied Polymer Science*, *133*(15). https://doi.org/10.1002/app.43286

Diaz-Rodríguez, K.F., Salazar-Pinto, B.M., Flores-Calla, S.S., & Gonzales-Condori, E.G. (2025). Potential use of artichoke (*Cynara cardunc*ulus L.) waste packed in filter bags for the removal of hexavalent chromium from water. *Revista Mexicana de Ingeniería Química 24*(1), IA25426. https://doi.org/10.24275/rmiq/IA25426

Elewa, A.M., Amer, A.A., Attallah, M.F., Gad, H.A., Al-Ahmed, Z.A.M. and Ahmed, I.A. (2023). Chemically activated carbon based on biomass for adsorption of Fe(III) and Mn(II) ions from aqueous solution. *Materials 16*, 1251. https://doi.org/10.3390/ma16031251

Febrianto, J., Kosasih, A. N., Sunarso, J., Ju, Y.-H., Indraswati, N., & Ismadji, S. (2009). Equilibrium and kinetic studies in adsorption of heavy metals using biosorbent: A summary of recent studies. *Journal of Hazardous Materials*, *162*(2–3), 616–645. https://doi.org/10.1016/j.jhazmat.2008.06.042

Flores-Trujillo, A. K. I., Mussali-Galante, P., de Hoces, M. C., Blázquez-García, G., Saldarriaga-Noreña, H. A., Rodríguez-Solís, A., … Ortiz-Hernández, L. (2021). Biosorption of heavy metals on Opuntia fuliginosa and *Agave angustifolia* fibers for their elimination from water. *International Journal of Environmental Science and Technology*, *18*(2), 441–454.

https://doi.org/10.1007/s13762-020-02832-8

Foo, K. Y., & Hameed, B. H. (2010). Insights into the modeling of adsorption isotherm systems. *Chemical Engineering Journal*, *156*(1), 2–10. https://doi.org/10.1016/j.cej.2009.09.013

Freundlich, H. (1906). Over the adsorption in solution. *J. Phys. Chem.*, *57*, 1100–1107.

Gómez-Navarro, C. S., Warren-Vega, W. M., Serna-Carrizales, J. C., Zárate-Guzmán, A. I., Ocampo-Pérez, R., Carrasco-Marín, F., Collins-Martínez, V. H., Niembro-García, J., & Romero-Cano, L. A. (2023). Evaluation of the environmental performance of adsorbent materials prepared from agave bagasse for water remediation: Solid waste management proposal of the tequila industry. *Materials*, *16*(1), 8. https://doi.org/10.3390/ma16010008

Grams, J. (2022). Surface analysis of solid products of thermal treatment of lignocellulosic biomass. *Journal of Analytical and Applied Pyrolysis*, *161*, 105429. https://doi.org/10.1016/j.jaap.2021.105429

Hernández-Francisco, E., Bonilla-Cruz, J., Márquez-Lamas, U., Suárez-Jacobo, Á., Longoria-Rodríguez, F., Rivera-Haro, J., …& Lara-Ceniceros, T. E. (2020). Entangled cellulose nanofibrils/nanosheets derived from native mexican agave for lead (II) ion removal. *Cellulose*, *27*(15), 8785–8798. https://doi.org/10.1007/s10570-020-03373-6

Hospodarova, V., Singovszka, E., & Stevulova, N. (2018). Characterization of cellulosic fibers by FTIR spectroscopy for their further implementation to building materials. *American Journal of Analytical Chemistry*, *9*(6), 303–310. https://doi.org/10.4236/ajac.2018.96023

Kaur, K., Kaur, R., & Kaur, H. (2024). A systematic review of lignocellulosic biomass for remediation of environmental pollutants. *Applied Surface Science Advances*, *19*, 100547. https://doi.org/10.1016/j.apsadv.2023.100547

Langmuir, I. (1918). The adsorption of gases on plane surfaces of glass, mica and platinum. *Journal of the American Chemical Society*, *40*(9), 1361–1403. https://doi.org/10.1021/ja02242a004

Lavado-Meza, C., De la Cruz-Cerrón, L., Cisneros-Santos, G., De la Cruz, A.H., Angeles-Suazo, J. & Dávalos-Prado, J.Z. (2023). Arabica-coffee and teobroma-cocoa agro-industrial waste biosorbents, for Pb(II) removal in aqueous solutions. *Environmental Science and Pollution Research* 30, 2991-3001. https://doi.org/10.1007/s11356-022-22233-3

López-González, H., Sánchez-Nava, D. M., & Olguín, M. T. (2022). *Agave salmiana* as biosorbent of cobalt and cobalt-nickel ionic species from aqueous solutions. *Desalination and Water Treatment*, *278*, 141–146. https://doi.org/10.5004/dwt.2022.29081

Luzardo, F. H. M., Velasco, F. G., Alves, C. P., Correia, I. K. da S., & Cazorla, L. L. (2015). Chemical characterization of agroforestry solid residues aiming its utilization as adsorbents for metals in water. *Revista Brasileira de Engenharia Agrícola e Ambiental*, *19*(1), 77–83. https://doi.org/10.1590/1807-1929/agriambi.v19n1p77-83

Majamo, S. L., Amibo, T. A., & Tsegaw, E. Z. (2024). Enhanced cellulose extraction from agave plant (*Agave americana* Species) for synthesis of magnetic/cellulose nanocomposite for defluoridation of water. *Materials Today Communications*, *38*, 107683. https://doi.org/10.1016/j.mtcomm.2023.107683

Martínez, S., Nuñez-Guerrero, M., Gurrola-Reyes, J. N., Rutiaga-Quiñones, O. M., Paredes-Ortíz, A., Soto, O. N., … Rodriguez-Herrera, R. (2019). Mescal an alcoholic beverage from Agave spp. with great commercial potential. *The Science of Beverages*, (In Alcoholic Beverages: Volume 7), (pp. 113–140). Elsevier. https://doi.org/10.1016/B978-0-12-815269-0.00004-0

Moreno-Rubio, J.G., Osornio-Rubio, N.R., Jiménez-Islas, H., Barrera-Calva, E., Ramírez-Yañez, A.Y., & Martínez-González, G.M. (2025). Characterization and efficiency of *Luffa cylindrica* as bioadsorbent in Cr(VI) remotion from synthetic wastewater. *Revista Mexicana de Ingeniería Química 24*(2), Mat25443. https://doi.org/10.24275/rmiq/Mat25443

Nighojkar, A., Zimmermann, K., Ateia, M., Barbeau, B., Mohseni, M., Krishnamurthy, S., … Kandasubramanian, B. (2023). Application of neural network in metal adsorption using biomaterials (BMs): a review. *Environmental Science: Advances*, *2*(1), 11–38. https://doi.org/10.1039/D2VA00200K

Perez-Pimienta, J. A., Méndez-Acosta, H. O., Davis, S. C., Kean, D., & Tan, Y. (2024). Editorial: The role of agave as feedstock within a sustainable

circular bioeconomy. *Frontiers in Chemical Engineering*, *5*, 1343629. https://doi.org/10.3389/fceng.2023.1343629

Pérez-Zavala, M. de L., Hernández-Arzaba, J. C., Bideshi, D. K., & Barboza-Corona, J. E. (2020). Agave: a natural renewable resource with multiple applications. *Journal of the Science of Food and Agriculture*, Vol. 100, pp. 5324–5333. John Wiley and Sons Ltd. https://doi.org/10.1002/jsfa.10586

Poonam, S.K.B. and Kumar, N. (2018). Kinetic study of lead (Pb^{2+}) removal from battery manufacturing wastewater using bagasse biochar as biosorbent. *Applied Water Science 8*, 119. https://doi.org/10.1007/s13201-018-0765-z

Prasad, B., Das, P., Srivastava, V., & Kumar, M. (2023). Perspectives of heavy metal pollution indices for soil, sediment, and water pollution evaluation: An insight. *Total Environment Research Themes*, *6*, 100039. https://doi.org/10.1016/j.totert.2023.100039

Rathnayaka, R. M. H., Priyantha, N., & Gunathilake, W. S. S. (2024). Colloids and Surfaces C: Environmental Aspects Removal of trivalent and hexavalent chromium from aqueous solution using fiber of *Agave americana* plant and its modified forms. *Colloids and Surfaces C: Environmental Aspects*, *2*, 100029. https://doi.org/10.1016/j.colsuc.2024.100029

Sánchez-Moreno, H., García-Rodríguez, L., & Recalde-Moreno, C. (2025). Natural cellulose fibers from *Agave americana* L. ASPARAGACEAE as an effective adsorbent for mercury in aqueous solutions. *Adsorption*, *31*(2), 40. https://doi.org/10.1007/s10450-024-00590-4

Santos, P. F., Neris, J. B., Heriberto, F., Luzardo, M., Velasco, F. G., Tokumoto, M. S., & Serpa, R. (2019). Chemical modification of four lignocellulosic materials to improve the Pb^{2+} and Ni^{2+} ions adsorption in aqueous solutions. *Journal of Environmental Chemical Engineering*, *7*(5), 103363. https://doi.org/10.1016/j.jece.2019.103363

Sharma, K., Rajan, S., & Nayak, S. K. (2024). Water pollution: Primary sources and associated human health hazards with special emphasis on rural areas. In *Water Resources Management for Rural Development* (First Edit, pp. 3–14). Elsevier. https://doi.org/10.1016/B978-0-443-18778-0.00014-3

Syeed, M. M. M., Hossain, S., Karim, R., Faisal, M., Hasan, M., & Hayat, R. (2023). Surface water quality profiling using the water quality index, pollution index and statistical methods: A critical review. *Environmental and Sustainability Indicators*, *18*, 100247. https://doi.org/10.1016/j.indic.2023.100247

Tejada-Tovar, C., Gonzalez-Delgado, A. D., & Villabona-Ortiz, A. (2019). Characterization of residual biomasses and its application for the removal of lead ions from aqueous solution. *Applied Sciences*, *9*(21), 4486. https://doi.org/10.3390/app9214486

Thakur, V., Sharma, E., Guleria, A., Sangar, S., & Singh, K. (2020). Modification and management of lignocellulosic waste as an ecofriendly biosorbent for the application of heavy metal ions sorption. *Materials Today: Proceedings*, *32*, 608–619. https://doi.org/10.1016/j.matpr.2020.02.756

Vázquez-Sánchez, A. Y., Lima, E. C., Abatal, M., Tariq, R., Santiago, A. A., Alfonso, I., … Vazquez-Olmos, A. R. (2023). Biosorption of Pb (II) Using Natural and Treated Ardisia compressa K. Leaves: Simulation Framework Extended through the Application of Artificial Neural Network and Genetic Algorithm. *Molecules*, *28*(17), 6387. https://doi.org/10.3390/molecules28176387

Velazquez-Jimenez, L. H., Pavlick, A., & Rangel-Mendez, J. R. (2013). Chemical characterization of raw and treated agave bagasse and its potential as adsorbent of metal cations from water. *Industrial Crops and Products*, *43*, 200–206. https://doi.org/10.1016/j.indcrop.2012.06.049

Vigdorowitsch, M., Pchelintsev, A., Tsygankova, L., & Tanygina, E. (2021). Freundlich isotherm: an adsorption model complete framework. *Applied Sciences*, *11*(17), 8078. https://doi.org/10.3390/app11178078

Xie, B., Hou, Y., & Li, Y. (2020). Modified lignin nanosphere adsorbent for lead and copper ions. *BioResources*, *16*(1), 249–262. https://doi.org/10.15376/biores.16.1.249-262

Yadav, M., Singh, N., Annu, Khan, S. A., Raorane, C. J., & Shin, D. K. (2024). Recent advances in utilizing lignocellulosic biomass materials as adsorbents for textile dye removal: a comprehensive review. *Polymers*, *16*(17), 2417. https://doi.org/10.3390/polym16172417

Zadehahmadi, F., Eden, N. T., Mahdavi, H., Konstas, K., Mardel, J. I., Shaibani, M., … Hill, M. R. (2023). Environmental Science Water Research & Technology Removal of metals from water using MOF-based composite adsorbents. *About Environmental Science: Water Research & Technology*, *9,* 1305–1330. https://doi.org/10.1039/d2ew00941b